

# Prediction of super-heavy $N^*$ and $\Lambda^*$ resonances with hidden beauty

Jia-Jun Wu<sup>1</sup>, Lu Zhao<sup>1</sup> and B. S. Zou<sup>1,2</sup>

<sup>1</sup> Institute of High Energy Physics, CAS, P.O.Box 918(4), Beijing 100049, China

<sup>2</sup> Theoretical Physics Center for Science Facilities, CAS, Beijing 100049, China

(Dated: June 26, 2011)

## Abstract

The meson-baryon coupled channel unitary approach with the local hidden gauge formalism is extended to the hidden beauty sector. A few narrow  $N^*$  and  $\Lambda^*$  resonances around 11 GeV are predicted as dynamically generated states from the interactions of heavy beauty mesons and baryons. Production cross sections of these predicted resonances in  $pp$  and  $ep$  collisions are estimated as a guide for the possible experimental search at relevant facilities.

## I. INTRODUCTION

In conventional quark models, all established baryons are ascribed into simple 3-quark (qqq) configurations [1]. The excited baryon states are described as excitation of individual constituent quarks, similar to the cases for atomic and nuclear excitations. However, unlike atomic and nuclear excitations, the typical hadronic excitation energies are comparable with constituent quark masses. Hence to drag out a  $q\bar{q}$  pair from gluon field could be a new excitation mechanism besides the conventional orbital excitation of original constituent quarks. Some baryon resonances are proposed to be meson-baryon dynamically generated states [2–8] or states with large ( $qqqq\bar{q}$ ) components [9–11]. A difficulty to pin down the nature of these baryon resonances is that the predicted states from various models are around the same energy region and there are always some adjustable ingredients in each model to fit the experimental data. A typical example is  $N^*(1535)$  which has large couplings to the strangeness. In the 3-quark (qqq) configurations, it is described as the orbital angular momentum  $L = 1$  excitation of a quark. But phenomenological studies suggest that it may be a quasi-bound state of  $K\Sigma$  system [12–14], or a hidden strangeness 5-quark state [10, 15]. In order to clearly demonstrate the new excitation mechanism with some of its corresponding states, in Ref.[16], the meson-baryon coupled channel unitary approach with the local hidden gauge formalism was performed for the hidden charm sector and several narrow  $N^*$  and  $\Lambda^*$  resonances with hidden charm were predicted to exist. If found experimentally, these resonances definitely could not be described as three constituent quark states. Here, we extend the study to the hidden beauty sector. Some super-heavy  $N^*$  and  $\Lambda^*$  resonances with hidden beauty are predicted to exist, with mass around 11 GeV and width smaller than 10 MeV. If these resonances would be experimentally confirmed, they should be part of the heaviest super-heavy island of  $N^*$  and  $\Lambda^*$  state. As a guild to the future experimental search for these new predicted states, their production cross sections in  $pp$  and  $ep$  collisions are estimated.

In the next section, we present the formalism and ingredients for the study of interactions between heavy beauty meson and baryon with the Valencia approach, and give some detailed discussion on the intermediate meson-baryon loop G functions. In section III, our numerical results for the masses and widths of the predicted super-heavy  $N^*$  and  $\Lambda^*$  states are given, followed by a discussion. In section IV, effects of momentum dependent terms in the effective

potential are investigated. In section V, the calculation about production of these predicted states from  $pp$  and  $ep$  collisions is presented. Finally, a short summary is given in the last section.

## II. FORMALISM FOR MESON-BARYON INTERACTION

We follow the recent work of Ref. [16] on the interactions between charmed mesons and baryons, and replace charm quark by beauty quark. The  $PB \rightarrow PB$  and  $VB \rightarrow VB$  interactions by exchanging a vector meson are considered, as shown by the Feynman diagrams in Fig. 1.

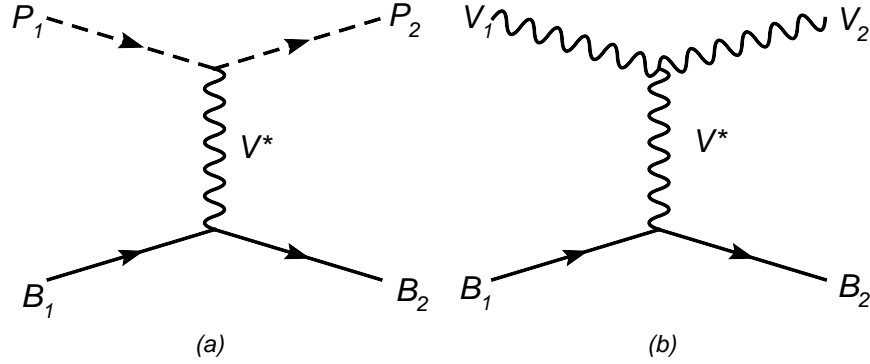


FIG. 1: Feynman diagrams for the pseudoscalar-baryon (a) or vector-baryon (b) interaction via the exchange of a vector meson ( $P_1, P_2$  are  $B^0, B^+$  or  $B_s^0$ , and  $V_1, V_2$  are  $B^{0*}, B^{+*}$  or  $B_s^{0*}$ , and  $B_1, B_2$  are  $\Sigma_b, \Lambda_b, \Xi_b, \Xi'_b$  or  $\Omega_b$ , and  $V^*$  is  $\rho, K^*, \phi$  or  $\omega$ ).

The effective Lagrangians for the interactions involved are [17]:

$$\begin{aligned}
 \mathcal{L}_{VVV} &= ig \langle V^\mu [V^\nu, \partial_\mu V_\nu] \rangle \\
 \mathcal{L}_{PPV} &= -ig \langle V^\mu [P, \partial_\mu P] \rangle \\
 \mathcal{L}_{BBV} &= g (\langle \bar{B} \gamma_\mu [V^\mu, B] \rangle + \langle \bar{B} \gamma_\mu B \rangle \langle V^\mu \rangle)
 \end{aligned} \tag{1}$$

where  $P$  and  $V$  stand for pseudoscalar and vector mesons of the 16-plet of  $SU(4)$ , respectively.

Using the same approach of Ref.[16], we keep only the  $\gamma^0$  component of Eq.(1), while the three momentum versus the mass of the meson can be neglected under the low energy approximation. Similarly, the  $q^2/M_V^2$  term in the vector meson propagator is neglected so that the propagator is approximately equal to  $g^{\mu\nu}/M_V^2$ . Note when we consider transitions

from heavy mesons to light ones later on, we perform the exact calculation without such approximation. Then with  $g = M_V/2f$  the transition potentials corresponding to the diagrams of Fig. 1 are given by

$$V_{ab(P_1 B_1 \rightarrow P_2 B_2)} = \frac{C_{ab}}{4f^2}(E_{P_1} + E_{P_2}), \quad (2)$$

$$V_{ab(V_1 B_1 \rightarrow V_2 B_2)} = \frac{C_{ab}}{4f^2}(E_{V_1} + E_{V_2})\vec{\epsilon}_1 \cdot \vec{\epsilon}_2, \quad (3)$$

where the  $a, b$  stand for different channels of  $P_1(V_1)B_1$  and  $P_2(V_2)B_2$ , respectively. The  $E$  is the energy of corresponding particle. The  $\vec{\epsilon}$  is the polarization vector of the initial or final vector. And the  $\epsilon_{1,2}^0$  component is neglected consistently with taking  $\vec{p}/M_V \sim 0$ , with  $\vec{p}$  the momentum of the vector meson. Here we only change the charm quark to beauty quark, so the  $C_{ab}$  coefficients are exactly the same as those in Ref.[16], so that there are only two cases,  $(I, S) = (1/2, 0)$  and  $(0, -1)$ , which have attractive potentials. We list the values of the  $C_{ab}$  coefficients for  $PB \rightarrow PB$  for these two cases in Table I and Table II, respectively.

TABLE I: Coefficients  $C_{ab}$  in Eq. (2) for  $(I, S) = (1/2, 0)$

	$B\Sigma_b$	$B\Lambda_b$	$\eta_b N$	$\pi N$	$\eta N$	$\eta' N$	$K\Sigma$	$K\Lambda$
$B\Sigma_b$	-1	0	$-\sqrt{3/2}$	-1/2	$-1/\sqrt{2}$	1/2	1	0
$B\Lambda_b$		1	$\sqrt{3/2}$	-3/2	$1/\sqrt{2}$	-1/2	0	1

TABLE II: Coefficients  $C_{ab}$  in Eq. (2) for  $(I, S) = (0, -1)$

	$B_s\Lambda_b$	$B\Xi_b$	$B\Xi'_b$	$\eta_b\Lambda$	$\pi\Sigma$	$\eta\Lambda$	$\eta'\Lambda$	$\bar{K}N$	$K\Xi$
$B_s\Lambda_b$	0	$-\sqrt{2}$	0	1	0	$\sqrt{\frac{1}{3}}$	$\sqrt{\frac{2}{3}}$	$-\sqrt{3}$	0
$B\Xi_b$		-1	0	$\sqrt{\frac{1}{2}}$	$-\frac{3}{2}$	$\sqrt{\frac{1}{6}}$	$-\sqrt{\frac{1}{12}}$	0	$\sqrt{\frac{3}{2}}$
$B\Xi'_b$			-1	$-\sqrt{\frac{3}{2}}$	$\sqrt{\frac{3}{4}}$	$-\sqrt{\frac{1}{2}}$	$\frac{1}{2}$	0	$\sqrt{\frac{1}{2}}$
$\eta_b\Lambda$				0	0	0	0	0	0

With the transition potential, the coupled-channel scattering matrix can be obtained by solving the coupled-channel Bethe-Salpeter equation in the on-shell factorization approach of Refs.[3, 5]

$$T = [1 - VG]^{-1}V \quad (4)$$

with  $G$  being the loop function of a meson (P), or a vector (V), and a baryon (B). The  $\vec{\epsilon}_1 \cdot \vec{\epsilon}_2$  factor of Eq. (3) factorizes out also in  $T$ .

For the  $G$  loop function, there are usually two ways to regularize it. The first one is using dimensional regularization by means of the formula

$$\begin{aligned}
G &= i2M_B \int \frac{d^4q}{(2\pi)^4} \frac{1}{(P-q)^2 - M_B^2 + i\epsilon} \frac{1}{q^2 - M_P^2 + i\epsilon}, \\
&= \frac{2M_B}{16\pi^2} \left\{ a_\mu + \ln \frac{M_B^2}{\mu^2} + \frac{M_P^2 - M_B^2 + s}{2s} \ln \frac{M_P^2}{M_B^2} \right. \\
&\quad + \frac{\bar{q}}{\sqrt{s}} \left[ \ln(s - (M_B^2 - M_P^2) + 2\bar{q}\sqrt{s}) + \ln(s + (M_B^2 - M_P^2) + 2\bar{q}\sqrt{s}) \right. \\
&\quad \left. \left. - \ln(-s - (M_B^2 - M_P^2) + 2\bar{q}\sqrt{s}) - \ln(-s + (M_B^2 - M_P^2) + 2\bar{q}\sqrt{s}) \right] \right\}, \quad (5)
\end{aligned}$$

where  $q$  is the four-momentum of the meson,  $P$  is the total four-momentum of the meson and the baryon,  $s = P^2$ ,  $\bar{q}$  denotes the three momentum of the meson or baryon in the center of mass frame,  $\mu$  is a regularization scale, which we put 1000 MeV here. Changes in the scale are reabsorbed in the subtraction constant  $a_\mu$  to make results scale independent.  $a_\mu$  is of the order of  $-2$ , which is the natural value of the subtraction constant [18]. When we look for poles in the second Riemann sheet, we should change  $q$  to  $-q$  when  $\sqrt{s}$  is above the threshold in Eq.(5) [19].

The second way to regularize the  $G$  loop function is by putting a cutoff in the three-momentum:

$$\begin{aligned}
G &= i2M_B \int \frac{d^4q}{(2\pi)^4} \frac{1}{(P-q)^2 - M_B^2 + i\epsilon} \frac{1}{q^2 - M_P^2 + i\epsilon} \\
&= \int_0^\Lambda \frac{\bar{q}^2 d\bar{q}}{4\pi^2} \frac{2M_B(\omega_P + \omega_B)}{\omega_P \omega_B (s - (\omega_P + \omega_B)^2 + i\epsilon)}, \quad (6)
\end{aligned}$$

where  $\omega_P = \sqrt{\bar{q}^2 + M_P^2}$ ,  $\omega_B = \sqrt{\bar{q}^2 + M_B^2}$ , and  $\Lambda$  is the cutoff parameter in the three-momentum of the function loop.

Here we give some detailed discussion on these two types of  $G$  function. Firstly the free parameters are  $a_\mu$  in Eq.(5) and  $\Lambda$  in Eq.(6). The value of  $\Lambda$  is around 0.8 GeV, which are within the natural range for effective theories [5]. Then the  $a_\mu$  parameter is determined by requiring that the two  $G$  functions from Eq.(5) and Eq.(6) take the same value at threshold. This value also leads to similar shape near threshold for the two  $G$  functions as shown in Fig.2. In Fig.2, the real part and imaginary part of two  $G$  functions vs the energy difference between the center mass energy and the corresponding threshold for  $K\Sigma$ ,  $\bar{D}\Sigma_c$

and  $B\Sigma_b$  channels are demonstrated. In Table.III, the parameters for different  $G$  functions and channels are listed. While the imaginary parts of two  $G$  functions are exactly the same, there are some differences for the real parts of two  $G$  functions and the differences become bigger for heavier channels. For the same  $\Lambda$  value, the magnitude of  $a_\mu$  depends on the threshold of channels and gets bigger for heavier channels. One point worth mentioning is that for the  $B\Sigma_b$  channel the real part of the  $G$  function given by Eq.(5) is larger than zero for energies more than 50 MeV below the threshold as shown in Fig.2. As we know, if the interaction is repulsive potential, *i.e.*, the value of the potential  $V$  is positive, there should be no bound state. However, when the real part of  $G$  function is also positive below the threshold, the pole can still be found in the model  $T$  matrix with a repulsive potential. These poles far below threshold are beyond the valid region of the model approximation and should be discarded. Since varying the  $G$  function in a reasonable range does not influence our conclusion qualitatively, we present our numerical results in the dimensional regularization scheme with  $a_\mu = -3.71$ , in this paper.

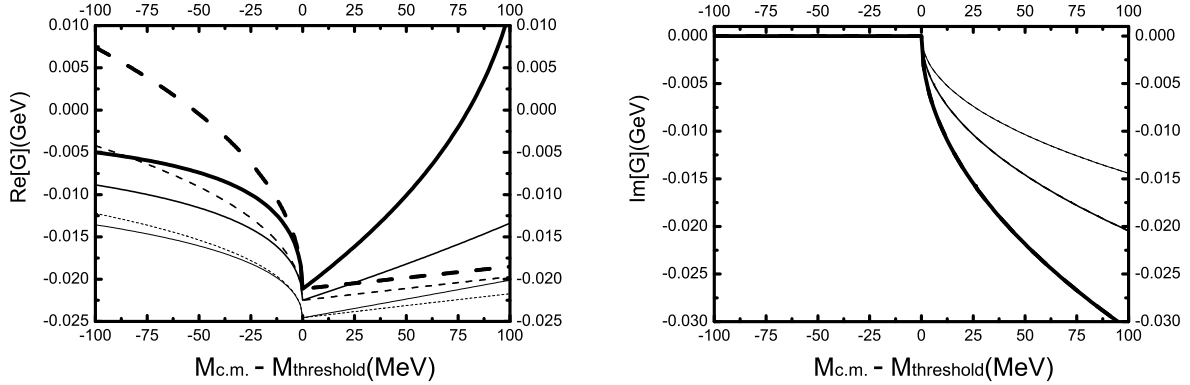


FIG. 2: The real part (left) and imaginary part (right) of two  $G$  functions vs the energy difference between the C.M. energy and the threshold energy. The solid lines are for Eq.(6), and dashed lines are for Eq.(5). The thickest lines are for  $B\Sigma_b$  channel, the thinnest ones are for  $K\Sigma$  channel, and middle ones are for  $\bar{D}\Sigma_c$  channel. The used parameters are listed in the Table.III with  $\Lambda = 0.8\text{GeV}$ .

With the potential and  $G$  function fixed, the unitary  $T$  amplitude can be obtained by Eq.(4). The poles in the  $T$  matrix are looked for in the complex plane of  $\sqrt{s}$ . Those appearing in the first Riemann sheet below threshold are considered as bound states whereas those located in the second Riemann sheet and above the threshold of some channel are identified

TABLE III: The parameters for two types of G functions in the cases of  $K\Sigma$ ,  $\bar{D}\Sigma_c$  and  $B\Sigma_b$  interactions, with  $a_\mu$  for Eq.(5) and  $\Lambda$  for Eq.(6). The listed  $a_\mu$  and  $\Lambda(\text{GeV})$  give the same value of two G functions at the corresponding threshold.

	Threshold(GeV)	$a_\mu$				
$\Lambda(\text{GeV})$		0.7	0.8	0.9	1.0	1.1
$B\Sigma_b$	11.087	-3.679	-3.715	-3.751	-3.786	-3.822
$\bar{D}\Sigma_c$	4.231	-2.196	-2.283	-2.369	-2.453	-2.536
$K\Sigma$	1.688	-1.297	-1.463	-1.619	-1.766	-1.905

as resonances. As previously discussed, the poles will be kept only when the real part of Eq.(5) is negative.

From the T matrix for the  $PB \rightarrow PB$  and  $VB \rightarrow VB$  coupled-channel systems, we can find the pole positions  $z_R$ . Six poles are found in the real axes below corresponding thresholds and therefore they are bound states. For these cases the coupling constants are obtained from the amplitudes in the real axis. These amplitudes behave close to the pole as:

$$T_{ab} = \frac{g_a g_b}{\sqrt{s} - z_R}. \quad (7)$$

We can use the residue of  $T_{aa}$  to determine the value of  $g_a$ , except for a global phase. Then, the other couplings are derived from

$$g_b = \lim_{\sqrt{s} \rightarrow z_R} \left( \frac{g_a T_{ab}}{T_{aa}} \right). \quad (8)$$

### III. NUMERICAL RESULTS FOR THE SUPER-HEAVY $N^*$ AND $\Lambda^*$

Firstly, we discuss the (I, S) = (1/2, 0) sector. There are two channels,  $B\Sigma_b$  and  $B\Lambda_b$ . The masses of these particles are taken from [1],  $m_B = 5.279$  GeV,  $m_{B^*} = 5.325$  GeV,  $m_{\Sigma_b} = 5.808$  GeV and  $m_{\Lambda_b} = 5.620$  GeV. With the approach outlined in the last section, the obtained pole positions  $z_R$  and coupling constants  $g_\alpha$  are listed in Tables IV for  $PB \rightarrow PB$  and  $VB \rightarrow VB$ . Because these poles are bound states for each channel, they have zero width when neglecting transitions mediated by t-channel exchange of heavy beauty mesons.

To consider some possible decay channels for them, such as  $\pi N$ ,  $\eta N$ ,  $K\Sigma$ ,  $\eta_b N$  and so on, we estimate these decays through heavy beauty meson exchanges by means of box diagrams as in Refs.[16, 20, 21]. We neglect transitions to the hidden charm channels such as  $\bar{D}\Sigma_c$  and  $\bar{D}\Lambda_c^+$ , because they need t-channel exchange of too heavy vector meson constituted of charm and beauty quarks. The results for  $PB$  and corresponding  $VB$  channels are listed in Table V. Comparing results in Table IV and Table V, the influence of these additional coupled channels to the masses of predicted states is negligible. This is because the transition potential by exchanging heavy beauty vector meson is much smaller than the potential by exchanging light vector meson.

TABLE IV: Pole positions  $z_R$  and coupling constants  $g_a$  for the states in  $(I, S) = (1/2, 0)$  sector.

$z_R$ (MeV)	$g_\alpha$	
	$B\Sigma_b$	$B\Lambda_b$
11052	2.05	0
	$B^*\Sigma_b$	$B^*\Lambda_b$
11100	2.02	0

TABLE V: Mass ( $M$ ), total width ( $\Gamma$ ), and partial decay widths ( $\Gamma_i$ ) for  $(I, S) = (1/2, 0)$  sector.

$M$ (MeV)	$\Gamma$ (MeV)	$\Gamma_i$ (MeV)				
		$\pi N$	$\eta N$	$\eta' N$	$K\Sigma$	$\eta_b N$
11052	1.38	0.10	0.21	0.11	0.42	0.52
		$\rho N$	$\omega N$	$K^*\Sigma$	$\Upsilon N$	
11100	1.33	0.09	0.30	0.39	0.51	

We also do not consider the coupled channel effect between  $VB$  and  $PB$  channels as in Ref.[16]. The reason is that the transition potentials  $PB \rightarrow VB$  are much smaller than the potentials of  $PB \rightarrow PB$  or  $VB \rightarrow VB$ . Taking  $B\Sigma_b \rightarrow B^*\Sigma_b$  through t-channel pion exchange as an example, the  $B^*\pi B$  coupling is proportional to  $(p_B - p_\pi)_\mu \varepsilon_{B^*}^\mu$  and is zero in the static limit which ignores the three momenta of mesons and assumes  $\varepsilon_{B^*}^\mu = (0, \vec{\varepsilon}_{B^*})$ . Going beyond the static limit will give a non-zero transition potential but still much smaller



than its diagonal partners. This has been demonstrated by the production rate of  $J/\psi/\eta_c$  from  $\bar{p}p$  collisions in Ref.[16]. The cross section for  $\bar{p}p \rightarrow \bar{p}pJ/\psi$  through  $\bar{D}\Sigma_c$  bound state is smaller than that for  $\bar{p}p \rightarrow \bar{p}p\eta_c$  by more than an order of magnitude for similar excess energies. Therefore, the coupled channel effect between  $VB$  and  $PB$  channels is expected to have negligible influence on our predicted states.

One problem associated to the beauty sector should be addressed here. As shown in Fig.2, the loop functions of the hidden beauty sector, calculated with the cut-off or with dimensional regularization, show a quite different energy dependence and cannot be made similar over a reasonable range of values, as is the case for the hidden strange sector. This is due to that the on-shell momentum in the beauty channel shows a much stronger energy dependence than in the lightest channel. The results listed in Tables IV,V are obtained in the dimensional regularization scheme, where the subtraction constant is adjusted to the value of the  $\Lambda = 0.8$  GeV cut-off loop-function at threshold. However, the binding energy is found to be about 35 MeV for the  $B\Sigma_b$  channel, which lies quite away of its threshold, where the real parts of the two loop functions are very different. This makes the choice of matching point for the two loop functions questionable. In order to get some feeling about the choice of the match point, it is also tried to match the two loop functions at 30 MeV below threshold. Then the regularization subtraction constant moves from -3.715 to -3.774, and the binding energy moves from 35 MeV to 59 MeV. If the  $\Lambda = 0.8$  GeV cut-off loop function is used directly, then the binding energy increases to 145 MeV. So the simple Valencia model for the beauty sector works not as good as for the hidden strange sector. The uncertainty for the concrete binding energies is quite large of the order of tens to a hundred MeV. But the qualitative conclusion for possible existence of bound state should be very solid.

Then we discuss the  $(I, S) = (0, -1)$  sector. There are 3 channels,  $B_s\Lambda_b$ ,  $B\Xi_b$  and  $B\Xi'_b$ . The masses of  $B$ ,  $B_s$ ,  $\Xi_b$  and  $\Lambda_b$  have been precisely measured and can be taken from Ref.[1].  $m_{B_s} = 5.366$  GeV,  $m_{B_s^*} = 5.4128$  GeV and  $m_{\Xi_b} = 5.7924$  GeV. The  $\Xi'_b$  has not been observed yet. Its mass has been predicted to be 5.922 GeV in Ref.[22] and 5.960 GeV in Ref.[23]. We choose a middle value 5.940 GeV in this paper. From Table II, the  $B\Xi'_b$  channel is decoupled from other two channels, so there should be a bound state for this channel, the same as corresponding vector-meson-baryon channel,  $B^*\Xi'_b$ . For this channel, the results are listed in Table VI.

For the coupled  $B_s\Lambda_b$  and  $B\Xi_b$  channels, the T matrix can be written as:

$$T = \frac{1}{1 - V'G_{B\Xi_b}} \begin{pmatrix} V_{B_s\Lambda_b \rightarrow B\Xi_b}^2 G_{B\Xi_b} & V_{B_s\Lambda_b \rightarrow B\Xi_b} \\ V_{B_s\Lambda_b \rightarrow B\Xi_b} & V' \end{pmatrix} \quad (9)$$

with  $V' = V_{B\Xi_b \rightarrow B\Xi_b} + V_{B_s\Lambda_b \rightarrow B\Xi_b}^2 G_{B_s\Lambda_b}$ .

The  $V'$  is negative and hence provides an attractive potential. For  $a_\mu = -3.71$ , one pole is found for the coupled-channel system, with mass between the two thresholds of  $B_s\Lambda_b$  (10.986 GeV) and  $B\Xi_b$  (11.071 GeV). The pole position depends on the value of  $a_\mu$  as demonstrated in Table VI and can move to below the  $B_s\Lambda_b$  threshold when the magnitude of  $a_\mu$  increases, such as for  $a_\mu = -3.82$  corresponding to the  $\Lambda = 1.1$  GeV.

TABLE VI: Pole positions  $z_R$  with different  $a_\mu$  for  $PB \rightarrow PB$  in (I, S) = (0, -1) sector.

$\Lambda(\text{GeV})$	$a_\mu$	$z_R$ (MeV)	
	$B_s\Lambda_b$ and $B\Xi_b$	$B\Xi'_b$	
0.7	-3.68	$11030 - 0.60i$	11198
0.8	-3.71	$11021 - 0.59i$	11191
0.9	-3.75	$11004 - 0.49i$	11178
1.0	-3.78	$10990 - 0.24i$	11167
1.1	-3.82	10970	11151

The coupling constants and the possible decay channels of these two resonances are listed in Tables VII and VIII for  $a_\mu = -3.71$ . Similarly, the results for the corresponding vector-meson-baryon channels are also listed in Tables VII and VIII for  $a_\mu = -3.71$ .

Totally two  $N^*$  and four  $\Lambda^*$  states are predicted to exist with masses above 11 GeV and very narrow widths of only a few MeV. The very narrow widths are due to the fact that all decays are tied to the necessity of the exchange of a heavy beauty vector meson because of hidden  $b\bar{b}$  components involved in these states, and hence are suppressed. If these predicted narrow  $N^*$  and  $\Lambda^*$  resonances with hidden beauty would be found, they definitely cannot be accommodated by quark models with three constituent quarks. Together with other possible  $N^*$  and  $\Lambda^*$  states of other quantum numbers with hidden beauty, they should form a super-heavy island of the heaviest masses for excited nucleons  $N^*$  and excited hyperons  $\Lambda^*$ .

TABLE VII: Pole positions  $z_R$  and coupling constants  $g_a$  for the states in (I, S) = (0, -1) sector for  $a_\mu = -3.71$ .

$z_R$ (MeV)	$g_\alpha$		
	$B_s\Lambda_b$	$B\Xi_b$	$B\Xi'_b$
11021 - 0.59 <i>i</i>	0.14 - 0.11 <i>i</i>	2.27 + 0.004 <i>i</i>	0
11191	0	0	1.92
	$B_s^*\Lambda_b$	$B^*\Xi_b$	$B^*\Xi'_b$
11069 - 0.59 <i>i</i>	0.14 - 0.12 <i>i</i>	2.24 + 0.005 <i>i</i>	0
11238	0	0	1.89

TABLE VIII: Mass ( $M$ ), total width ( $\Gamma$ ), and partial decay widths ( $\Gamma_i$ ) for the states in (I, S) = (0, -1) sector for  $a_\mu = -3.71$ .

$M$ (MeV)	$\Gamma$ (MeV)	$\Gamma_i$ (MeV)						
		$\bar{K}N$	$\pi\Sigma$	$\eta\Lambda$	$\eta'\Lambda$	$K\Xi$	$\eta_b\Lambda$	$B_s\Lambda_b$
11021	2.21	0.65	0.01	0.08	0.14	0.01	0.19	1.18
11191	1.24	0	0.28	0.18	0.10	0.18	0.48	0
		$\bar{K}^*N$	$\rho\Sigma$	$\omega\Lambda$	$\phi\Lambda$	$K^*\Xi$	$\Upsilon\Lambda$	$B_s^*\Lambda_b$
11070	2.17	0.61	0.01	0.01	0.20	0.01	0.19	1.18
11239	1.19	0	0.26	0.26	0	0.17	0.48	0

#### IV. EFFECTS OF MOMENTUM DEPENDENT TERMS IN THE POTENTIAL

For our model calculations in the last two sections, the static limit is assumed for the t-channel exchange of light vector mesons by neglecting momentum dependent terms as discussed after the Eq.(1). However, in Ref.[24], dynamically generated open charmed baryons were studied by solving the Lippmann - Schwinger equation beyond the zero range approximation. The momentum dependent terms were found to have non-negligible effects on the results. In order to investigate the possible influence of the momentum dependent terms in this case, in this section, we use the conventional Schrodinger Equation approach to study

possible bound states for the  $B\Sigma_b$  channel by keeping the momentum dependent terms in the t-channel meson exchange potential.

The deduction of the momentum dependent potential by the t-channel exchange of light vector mesons is straightforward. By keeping momentum dependent terms up to quadratic order with proper normalization factor for the Schrodinger Equation and including the vertex form factors as in the Bonn potential model [25], the effective S-wave  $B\Sigma_b$  potential is obtained as the following:

$$V_{ab(P_1 B_1 \rightarrow P_2 B_2)}^S = \frac{C_{ab} m_V^2}{4f^2} \frac{1}{\vec{q}^2 + m_V^2} \left( \frac{\Lambda_V^2 - m_V^2}{\Lambda_V^2 + \vec{q}^2} \right)^2 \times \left( 1 + \frac{m_P^2 + 2m_B^2 + 4m_P m_B}{4m_P^2 m_B^2} \vec{k}^2 + \frac{2m_B^2 - m_P^2}{16m_P^2 m_B^2} \vec{q}^2 \right), \quad (10)$$

where  $\vec{k}$  and  $\vec{q}$  are defined as  $(\vec{p} + \vec{p}')/2$  and  $\vec{p} - \vec{p}'$  with  $\vec{p}$  and  $\vec{p}'$  the initial and final momenta of the pseudo-scalar meson, respectively, in the center of mass system of the  $B\Sigma_b$  channel. For simplicity, we assume the same cut-off parameter  $\Lambda_V$  for the  $\rho$  and  $\omega$  mesons.

The effective potential for the Schrodinger Equation in the coordinate space,  $V(\vec{r})$ , can be obtained by using the following Fourier-transformation formulae:

$$\begin{aligned} \mathcal{F}\left\{\left(\frac{\Lambda^2 - m^2}{\Lambda^2 + \vec{q}^2}\right)^2 \frac{1}{\vec{q}^2 + m^2}\right\} &= \frac{1}{4\pi} \left( \frac{e^{-mr}}{r} - \frac{e^{-\Lambda r}}{r} - (\Lambda^2 - m^2) \frac{e^{-\Lambda r}}{2\Lambda} \right), \\ \mathcal{F}\left\{\left(\frac{\Lambda^2 - m^2}{\Lambda^2 + \vec{q}^2}\right)^2 \frac{\vec{q}^2}{\vec{q}^2 + m^2}\right\} &= \frac{1}{4\pi} \left( m^2 \left( -\frac{e^{-mr}}{r} + \frac{e^{-\Lambda r}}{r} \right) + (\Lambda^2 - m^2) \frac{\Lambda e^{-\Lambda r}}{2} \right), \\ \mathcal{F}\left\{\left(\frac{\Lambda^2 - m^2}{\Lambda^2 + \vec{q}^2}\right)^2 \frac{\vec{k}^2}{\vec{q}^2 + m^2}\right\} &= \frac{1}{4\pi} \left( \frac{m^2}{4} \frac{e^{-mr}}{r} - \frac{\Lambda^2}{4} \frac{e^{-\Lambda r}}{r} - \frac{\Lambda^2 - m^2}{4} \left( \frac{\Lambda r}{2} - 1 \right) \frac{e^{-\Lambda r}}{r} \right) \\ &\quad - \frac{1}{8\pi} \left\{ \nabla^2, \frac{e^{-mr}}{r} - \frac{e^{-\Lambda r}}{r} - \frac{\Lambda^2 - m^2}{2} \frac{e^{-\Lambda r}}{\Lambda} \right\}. \end{aligned}$$

Then we can solve the Schrodinger Equation

$$\left( -\frac{\hbar^2}{2\mu} \nabla^2 + V(\vec{r}) - E \right) \Psi(\vec{r}) = 0, \quad (11)$$

to find possible bound state with eigenvalue  $E$  and corresponding wave function  $\Psi(\vec{r})$ , and estimate the size of the system  $\bar{r}$  with the formula

$$\bar{r} = \sqrt{\int r^2 dr d\Omega \Psi^*(\vec{r}) r^2 \Psi(\vec{r})}. \quad (12)$$

It is found that whether there exists a bound state depends on the cut-off parameter  $\Lambda_V$ . The results corresponding to various  $\Lambda_V$  values are listed in Table.IX.

TABLE IX: Eigenvalue  $E$  and average size of system  $\bar{r}$  vs the cut-off parameter  $\Lambda_V$ .

$\Lambda_V(\text{MeV})$	1100	1200	1300	1400	1500	1600	1700	1800	1900	2000
$E(\text{MeV})$	-	-0.85	-4.49	-10.5	-18.4	-27.9	-38.7	-50.5	-63.3	-78.9
$\bar{r}(\text{fm})$	-	2.36	1.19	0.86	0.70	0.60	0.53	0.48	0.44	0.41

From the Table IX, we can see that when the cut-off parameter  $\Lambda_V$  is 1200 MeV or larger, the effective potential can provide enough attraction to form a bound state. For  $\Lambda_V$  in the range of 1200  $\sim$  1800 MeV, the binding energy is in the range of 1  $\sim$  50 MeV with the average distance between two hadrons to be about 0.5  $\sim$  2 fm. The typical values for  $\Lambda_V$  in the Bonn potential are  $\Lambda_\rho = 1400$  MeV and  $\Lambda_\omega = 1500$  MeV [25]. The binding energy corresponding to  $\Lambda_V = 1600$  MeV is quite close to that obtained by the Valencia approach in the last section. This gives some justification of the simple Valencia approach although there could be an uncertainty of 10  $\sim$  20 MeV for the binding energy.

According to Ref.[26], “the apparent radius of the pion as seen by the photon is determined almost completely by the intermediate  $\rho$  meson: the intrinsic pion size must be considerably smaller than the measured charge radius. In descriptions which explicitly include the  $\rho$  meson, the pion can therefore be considered point-like for all practical purposes”. In our approach with the t-channel  $\rho$  meson exchange explicitly included, the D meson similar to the pion is expected to have very small size while the intrinsic radius of  $\Sigma_c$  baryon is expected to be around 0.5 fm similar to that for the proton [26]. With typical size  $\bar{r}$  larger than 0.5 fm, our predicted hadron molecular state should not suffer much from internal structure of the constituents.

For the  $B_s\Lambda_b$ - $B\Xi_b$  coupled channel case, it is not so easy to use the Schrodinger Equation approach. Since the simple Valencia approach gives a consistent result for the  $B\Sigma_b$  single channel case with Schrodinger Equation approach, we expect it also gives reasonable results for the  $B_s\Lambda_b$ - $B\Xi_b$  coupled channel case.

## V. PRODUCTION OF $N_{bb}^*$ AND $\Lambda_{bb}^*$ IN $pp$ AND $ep$ COLLISIONS

In order to look for these predicted super-heavy  $N_{bb}^*$  and  $\Lambda_{bb}^*$  states, we give an estimation of their production cross sections in the  $pp \rightarrow pp\eta_b$  and  $ep \rightarrow ep\Upsilon$  reactions. The Feynman

diagrams are shown in Fig.3. We also estimate the background of the  $pp \rightarrow pp\eta_b$  with  $N_{bb}^*$  replaced by the nucleon pole.

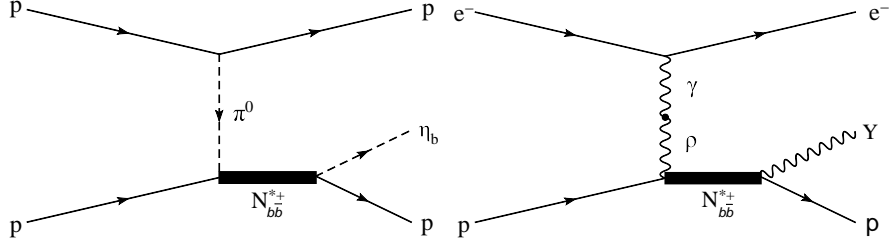


FIG. 3: Feynman diagrams for the reaction  $pp \rightarrow pp\eta_b$  and  $ep \rightarrow ep\Upsilon$ .

The Lagrangians for the interaction vertices of these two reactions are as follows [27–29]:

$$\mathcal{L}_{NN\pi} = g_{NN\pi} \bar{N} \gamma_5 \vec{\tau} \cdot \vec{\psi}_\pi N + h.c., \quad (13)$$

$$\mathcal{L}_{NN\eta_b} = g_{NN\eta_b} \bar{N} \gamma_5 \psi_{\eta_b} N + h.c., \quad (14)$$

$$\mathcal{L}_{N_{bb}^* N \pi} = g_{N_{bb}^* N \pi} \overline{N_{bb}^*} N \vec{\tau} \cdot \vec{\psi}_\pi + h.c., \quad (15)$$

$$\mathcal{L}_{N_{bb}^* N \eta_b} = g_{N_{bb}^* N \eta_b} \overline{N_{bb}^*} N \psi_{\eta_b} + h.c., \quad (16)$$

$$\mathcal{L}_{ee\gamma} = ie \bar{\psi}_e \gamma_\mu \psi_e A_\gamma^\mu + h.c., \quad (17)$$

$$\mathcal{L}_{\rho\gamma} = \frac{em_\rho^2}{f_\rho} \rho^\mu A_{\gamma\mu} + h.c., \quad (18)$$

$$\mathcal{L}_{N_{bb}^* N \rho} = g_{N_{bb}^* N \rho} \overline{N_{bb}^*} \gamma_5 \gamma^\mu N \tilde{g}_{\mu\nu}(P_{N_{cc}^*}) \vec{\tau} \cdot \vec{\psi}_\rho^\nu + h.c., \quad (19)$$

$$\mathcal{L}_{N_{bb}^* N \Upsilon} = g_{N_{bb}^* N \Upsilon} \overline{N_{bb}^*} \gamma_5 \gamma^\mu N \tilde{g}_{\mu\nu}(P_{N_{cc}^*}) \psi_\Upsilon^\nu + h.c.. \quad (20)$$

with  $\tilde{g}_{\mu\nu}(P) = -g_{\mu\nu} + \frac{P^\mu P^\nu}{P^2}$ .

In our model calculation, we only consider S-wave PB and VB interactions, so the spin-parity  $J^P$  of our predicted  $N_{bb}^*$  for the PB channels is  $1/2^-$ , and the  $N_{bb}^*$  for the VB channels can be either  $1/2^-$  or  $3/2^-$ , but assumed to be  $1/2^-$  here for a simple estimation of rough production rate. The coupling constants of the Lagrangians can be either calculated from its corresponding partial decay widths or obtained from references. They are all listed in Table X. For the  $NN\eta_b$  vertex, the width of  $\eta_b$  has not been measured. Since both  $\eta_b$  and  $\eta_c$  couple to nucleon through two gluon exchange, we use the relation  $g_{NN\eta_b} \sim g_{NN\eta_c} \alpha_s^4(M_{\eta_b}) / \alpha_s^4(M_{\eta_c})$  to estimate the  $g_{NN\eta_b}$  with  $g_{NN\eta_c}$  determined from the decay width of  $\eta_c \rightarrow p\bar{p}$ .

TABLE X: The coupling constants of involved vertices and corresponding widths used.

Vertex	$\Gamma(MeV)$	Coupling Constant( $g^2/4\pi$ )
$pp\pi^0$		14.4
$N_{bb}^{*+}p\pi^0$	0.033	$1.03 \times 10^{-5}$
$N_{bb}^{*+}p\eta_b$	0.52	$1.81 \times 10^{-3}$
$ee\gamma$		1/137
$\gamma\rho$		2.7 [27]
$N_{bb}^{*+}p\rho^0$	0.030	$1.55 \times 10^{-8}$
$N_{bb}^{*+}p\Upsilon$	0.51	$4.72 \times 10^{-4}$
$pp\eta_b$		$1 \times 10^{-6}$

As usual, the off-shell form factors should be considered here. We use two kinds of form factors for mesons and baryons, respectively.

$$F_M = \frac{\Lambda_M^2 - m_M^2}{\Lambda_M^2 - p_M^2}, \quad (21)$$

$$F_N = \frac{\Lambda_N^4}{\Lambda_N^4 + (p_N^2 - m_N^2)^2}, \quad (22)$$

where  $M$  stands for  $\pi$  or  $\rho$ , and  $N$  stands for  $N_{bb}^*$  or nucleon pole. Here  $\Lambda_M = 1.3$  GeV,  $\Lambda_N = 1.0$  GeV.

To produce the predicted  $N_{bb}^*(11052)$  in the pp collisions, the center-of-mass energy should be above 12 GeV. In Fig.4, the left figure shows our theoretical estimated total cross section for the  $pp \rightarrow pp\eta_b$  reaction through the  $N_{bb}^*$  production vs the center-of-mass energy, with (dashed curve) and without (solid curve) including the off-shell form factors. As an estimation of background contribution to the  $N_{bb}^*$  production, we also calculate the corresponding cross section through the off-shell nucleon pole without including the form factors. The result is shown by the dotted curve. The contribution from the nucleon pole is much smaller than that from the  $N_{bb}^*$  production, because the nucleon pole is much more off-shell than  $N_{bb}^*$ . The contribution of the nucleon pole with form factors becomes very small for the same reason, so it is not shown in Fig.4. This background reaction will not influence the observation of the  $N_{bb}^*$  production, especially for the energy range of  $13 \sim 25$  GeV. The cross section from  $N_{bb}^*$  production is about 0.1 nb, which is much smaller than that for the corresponding reaction  $pp \rightarrow pp\eta_c$  with  $N_{cc}^*$  production [16] of about  $0.1 \mu b$ . The main rea-

son is that both couplings of  $N_{bb}^*N\pi$  and  $N_{bb}^*N\eta_b$  are much smaller than the corresponding  $N_{cc}^*N\pi$  and  $N_{cc}^*N\eta_c$  couplings. These two vertices cause a reduction of about 2 orders of magnitude. In addition, because the center-of-mass energy here is much larger than that in the previous calculation for the  $\eta_c$  production, the propagator of exchanged  $\pi^0$  further reduces the contribution. For the same reason, the contribution with form factors is much less than that without them.

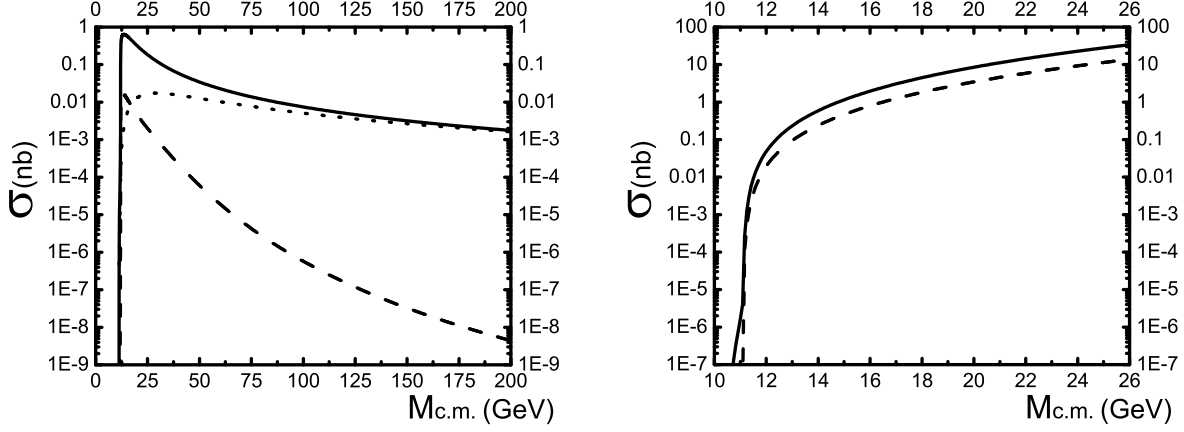


FIG. 4: Total cross section vs invariant mass of system for  $pp \rightarrow pp\eta_b$  reaction (left) and  $e^-p \rightarrow e^-p\Upsilon$  reaction (right), with (dashed curves) and without (solid curves) including off-shell form factors, through production of the predicted  $N_{bb}^*$  resonances. The dotted curve is the background contribution from the nucleon pole for the  $pp \rightarrow pp\eta_b$  reaction without including form factors.

For the production of  $N_{bb}^*(11100)$  in  $ep$  collisions, the invariant mass of the system should be above 11 GeV. The right figure in Fig.4 shows our calculated total cross section for the  $e^-p \rightarrow e^-p\Upsilon$  reaction vs the invariant mass of the system with (dashed curve) and without (solid curves) including form factors. The cross section of this reaction is much larger than that for the  $pp \rightarrow pp\eta_b$  reaction. The reason is due to the propagator of massless photon. The propagator of photon is given as the following:

$$\frac{1}{p_\gamma^2} = \frac{1}{2(m_e^2 + p_i p_f \cos\theta - E_i E_f)}, \quad (23)$$

where the  $p_i$ ,  $E_i$  are the three-momentum and energy of initial  $e^-$ , and  $p_f$ ,  $E_f$  for final  $e^-$ .  $\theta$  is the angle between initial and final  $e^-$ . When the directions of initial and final  $e^-$  are the same, i.e.,  $\cos\theta = 1$ , the value of Eq.(23) becomes very large because of the very small mass



of  $e^-$ . As the beam momentum of  $e^-$  becomes larger, the propagator of photon can reach very big value. For the invariant mass of the system less than 15 GeV, the cross section of  $e^-p \rightarrow e^-p\Upsilon$  reaction is of the same order of magnitude as that of  $pp \rightarrow pp\eta_b$  reaction.

## VI. SUMMARY

In summary, the meson-baryon coupled channel unitary approach with the local hidden gauge formalism is extended to the hidden beauty sector. Two  $N_{b\bar{b}}^*$  states and four  $\Lambda_{b\bar{b}}^*$  states are predicted to be dynamically generated from coupled PB and VB channels with the same approach as for the hidden charm sector [16]. Because of the hidden  $b\bar{b}$  components involved in these states, the masses of these states are all above 11 GeV while their widths are of only a few MeV, which should form part of the heaviest island for the quite stable  $N^*$  and  $\Lambda^*$  baryons. The nature of these states is similar as corresponding  $N_{c\bar{c}}^*$  and  $\Lambda_{c\bar{c}}^*$  states predicted in Ref.[16], which definitely cannot be accommodated by the conventional 3q quark models.

Production cross sections of the predicted  $N_{b\bar{b}}^*$  resonances in  $pp$  and  $ep$  collisions are estimated as a guide for the possible experimental search at relevant facilities in the future. For the  $pp \rightarrow pp\eta_b$  reaction, the best center-of-mass energy for observing the predicted  $N_{b\bar{b}}^*$  is  $13 \sim 25$  GeV, where the production cross section is about 0.01 nb. For the  $e^-p \rightarrow e^-p\Upsilon$  reaction, when the center-of-mass energy is larger than 14 GeV, the production cross section should be larger than 0.1 nb. Nowadays, the luminosity for pp or ep collisions can reach  $10^{33}cm^{-2}s^{-1}$ , this will produce more than 1000 events per day for the  $N_{b\bar{b}}^*$  production. We expect future facilities, such as proposed electron-ion collider (EIC) [30], to discover these very interesting super-heavy  $N^*$  and  $\Lambda^*$  with hidden beauty.

## Acknowledgments

This work is supported by the National Natural Science Foundation of China (NSFC) under grants Nos. 10875133, 10821063, 11035006 and by the Chinese Academy of Sciences under project No. KJCX2-EW-N01, and by the Ministry of Science and Technology of

- [1] Particle Data Group, K. Nakamura *et al.*, J. Phys. G **37**, 075021 (2010).
- [2] N. Kaiser, P. B. Siegel and W. Weise, Phys. Lett. B **362**, 23 (1995).
- [3] E. Oset and A. Ramos, Nucl. Phys. A **635**, 99 (1998).
- [4] J. A. Oller, E. Oset and A. Ramos, Prog. Part. Nucl. Phys. **45**, 157 (2000).
- [5] J. A. Oller and U. G. Meissner, Phys. Lett. B **500**, 263 (2001).
- [6] T. Inoue, E. Oset and M. J. Vicente Vacas, Phys. Rev. C **65**, 035204 (2002)
- [7] C. Garcia-Recio, M. F. M. Lutz and J. Nieves, Phys. Lett. B **582**, 49 (2004).
- [8] T. Hyodo, S. I. Nam, D. Jido and A. Hosaka, Phys. Rev. C **68**, 018201 (2003)
- [9] C. Helminen and D. O. Riska, Nucl. Phys. A **699**, 624 (2002).
- [10] B. C. Liu, B. S. Zou, Phys. Rev. Lett. **96**, 042002 (2006); *ibid*, **98**, 039102 (2007).
- [11] B. S. Zou, Nucl. Phys. A **835**, 199 (2010).
- [12] N. Kaiser, P. B. Siegel and W. Weise, Phys. Lett. B **362**, 23 (1995) [arXiv:nucl-th/9507036].
- [13] T. Inoue, E. Oset and M. J. Vicente Vacas, Phys. Rev. C **65**, 035204 (2002) [arXiv:hep-ph/0110333].
- [14] J. Nieves and E. Ruiz Arriola, Phys. Rev. D **64**, 116008 (2001)
- [15] L. S. Geng, E. Oset, B. S. Zou and M. Doring, Phys. Rev. C **79**, 025203 (2009) [arXiv:0807.2913 [hep-ph]].
- [16] J. J. Wu, R. Molina, E. Oset and B. S. Zou, Phys. Rev. Lett. **105** (2010) 232001, arXiv:1007.0573[nucl-th]; Phys. Rev. C **84** (2011) 015202, arXiv:1011.2399 [nucl-th].
- [17] E. Oset and A. Ramos, Euro. Phys. J. A **44**, 445 (2010).
- [18] J. A. Oller and U. G. Meissner, Phys. Lett. B **500**, 263 (2001) .
- [19] L. Roca, E. Oset and J. Singh, Phys. Rev. D **72**, 014002 (2005)
- [20] R. Molina, D. Nicmorus and E. Oset, Phys. Rev. D **78**, 114018 (2008)
- [21] L. S. Geng and E. Oset, Phys. Rev. D **79**, 074009 (2009)
- [22] Z. G. Wang, Phys. Lett. B **685**, 59 (2010) [arXiv:0912.1648 [hep-ph]].
- [23] E. E. Jenkins, Phys. Rev. D **54**, 4515 (1996) [arXiv:hep-ph/9603449].
- [24] C. E. Jimenez-Tejero, A. Ramos and I. Vidana, Phys. Rev. C **80**, 055206 (2009).
- [25] R. Machleidt, K. Holinde and C. Elster, Phys. Rept. **149**, 1 (1987).

- [26] T. E. O. Ericson and W. Weise, “PIONS AND NUCLEI,” *OXFORD, UK: CLARENDON*  
(1988) 479 P. (*THE INTERNATIONAL SERIES OF MONOGRAPHS ON PHYSICS*, 74)
- [27] J. J. Xie, C. Wilkin and B. S. Zou, Phys. Rev. C **77**, 058202 (2008) [arXiv:0802.2802 [nucl-th]].
- [28] B. S. Zou and F. Hussain, Phys. Rev. C **67**, 015204 (2003) [arXiv:hep-ph/0210164].
- [29] J. J. Wu, Z. Ouyang and B. S. Zou, Phys. Rev. C **80**, 045211 (2009).
- [30] V. Ptitsyn, AIP Conf. Proc. **1149**, 735 (2009).